



Article

Analysis of Characteristics for Inter-System Bias on Multi-GNSS Undifferenced and Uncombined Precise Point Positioning

Yangyang Lu, Hu Yang , Bo Li *, Jun Li, Aigong Xu and Mingze Zhang

School of Geomatics, Liaoning Technical University (LNTU), Fuxin 123000, China

* Correspondence: 471810031@stu.lntu.edu.cn

Abstract: Multi Global Navigation Satellite System (GNSS) Precise Point Positioning (PPP) has become the mainstream of PPP technology. Due to the differences in the coordinates and time references of each GNSS, multi-GNSS PPP must include additional Inter-System Bias (ISB) parameters to ensure compatibility between different GNSSs. Therefore, research on the characteristics of ISB is also essential. To analyze the short- and long-term time characteristics of multi-GNSS ISBs, as well as their relationship with receiver type and receiver antenna type, the Undifferenced and Uncombined (UDUC) PPP model of Global Positioning System (GPS), BeiDou navigation satellite system (BDS), and Galileo satellite navigation system (Galileo) was rigorously derived, and the physical of ISBs was elaborated in depth. ISB parameters were estimated and analyzed using 31 days of data from the 31 Multi-GNSS Experimental stations (MGEX). The results indicate that: (1) the ISB value is dependent on the station receiver type, receiver antenna type, analysis center product utilized, and GNSS system. (2) The short-term time characteristics of ISB-COM, ISB-WUM, and ISB-GBM are similar for the same station but not for the long term. In addition, ISBs are more stable in the short term. (3) There is little correlation between the ISB time characteristics, the receiver type, and the receiver antenna type, and the day-boundary discontinuity (DBD) on the ISB can be ignored for the consecutive days' process.

Keywords: precise point positioning; inter-system bias; multiple GNSSs; undifferenced and uncombined; characteristic analysis



Citation: Lu, Y.; Yang, H.; Li, B.; Li, J.; Xu, A.; Zhang, M. Analysis of Characteristics for Inter-System Bias on Multi-GNSS Undifferenced and Uncombined Precise Point Positioning. *Remote Sens.* **2023**, *15*, 2252. <https://doi.org/10.3390/rs15092252>

Academic Editors: Michael E. Gorbunov, Guanwen Huang, Liang Chen, Huizhong Zhu and Zhiguo Deng

Received: 29 March 2023

Revised: 18 April 2023

Accepted: 22 April 2023

Published: 24 April 2023



Copyright: © 2023 by the authors. Licensee MDPI, Basel, Switzerland. This article is an open access article distributed under the terms and conditions of the Creative Commons Attribution (CC BY) license (<https://creativecommons.org/licenses/by/4.0/>).

1. Introduction

With the rapid development of the Global Navigation Satellite System, it has formed the coexisting situation of GPS, GLONASS, Galileo, and BDS. There are currently more than 120 satellites in orbit, with the launch of the BDS-3 global positioning service contributing 30 satellites. It has substantially expanded the number of satellites in the global navigation satellite system [1]. Multi-GNSS provides users with a large amount of observation data, which is conducive to enhancing the geometry of observation, the accuracy of navigation and positioning, and the availability, continuity, reliability, accuracy, and integrity of navigation and positioning services [2,3]. Therefore, the fusion of multi-GNSS data has become the most significant challenge for GNSS applications.

The development of multi-frequency and multi-GNSS has enhanced the availability and scalability of PPP positioning technology, but it has also introduced some challenges. When positioning is integrated among GNSSs, the influence of inter-system differences must be considered due to the different coordinates and time datum of the global navigation system established by different countries. In the fusion of multi-GNSS observation data, we must consider not only the differences in the system time frame and coordinate system but also the impact of receiver hardware delay [4–6]. This difference, known as Inter-System Bias (ISB), has become the most significant concern in the integration and application of multi-GNSS observation data [5,6]. The incorporation of the ISB parameter into the

precision positioning of multi-GNSS fusion is conducive to strengthening the PPP model and enhancing the positioning precision [7,8]. In PPP, ISB is generally used as an additional parameter of the positioning model for estimation and calibration. To separate the phase ISB from ambiguity parameters, the pseudorange observation is generally used to initialize the phase ISB, and the observation model with conditions is used [8–11]. Many scholars on ISB have studied the processing strategy of parameter theory [7–10]. Jiang, Li, Zhang, Lu, and Zhou, as well as other scholars, have studied and analyzed ISB parameter estimation methods and stochastic models [11–15]. However, most of these studies are based on the analysis of single-day data processing results, and there are few studies on the results of the consecutive days' data processing.

Currently, an increasing number of researchers are interested in utilizing PPP technology to analyze and study the time characteristics of ISBs to resolve the ISB problem in multi-frequency multi-GNSS fusion positioning. Liu et al. proposed a multi-GNSS UDUC PPP model, studied the characteristics of ISBs in multi-GNSS, and analyzed the ISB characteristics among GPS, GLONASS, and BDS, but the analysis of the Galileo system was absent [16]. Chen et al. demonstrated that ISBs could be absorbed by clock shift parameters and ambiguity parameters [17–19]. El-Mowafy elaborated on the causes of ISB formation but did not investigate ISB characteristics [20]. Torre and Caporali demonstrated that the receiver hardware delay is related to the receiver antenna, but the receiver manufacturer does not offer a correction for this delay [21]. Meanwhile, Dach and Chen et al. studied the ISBs of various receivers, demonstrating that even identical receivers can have different hardware delays [22,23]. Gioia et al. calculated the ISB values of GPS, GLONASS, and Galileo by pseudorange and compared the differences of ISBs between different receivers, but the accuracy was poor, and research on BDS was lacking [24]. Zeng et al. investigated the ISB of a BDS/GPS pseudorange combination and discovered that it is affected by the system time difference, coordinate system difference, and receiver hardware delay [25].

At the same time, as GNSS system modernization progressed, the old and new systems adopted different architectural design concepts due to scientific and technological constraints at the time, particularly the research on ISB between the BDS-2 and BDS-3 systems. In addition, most studies examined and compared the BDS system as a single system. BDS-2 and BDS-3 modify and upgrade the signal's modulation and characteristics (B1I/B3I), which results in a difference in the reception and processing of BDS-2 (B1I/B3I) and BDS-3 (B1I/B3I) signals. Therefore, BDS-2 and BDS-3 are incompatible at the receiving end's hardware unit and baseband algorithm. Hence, ISB must be considered when B1I and B3I signals are used for BDS-2 and BDS-3 fusion PPP positioning [26]. In addition, most studies concentrate on analyzing the results of a single day, and the results of multiple days are primarily obtained by analyzing the results of consecutive single days, which does not accurately reflect the real long-term time characteristics of ISBs. Moreover, the studies on the relationship between ISB and receiver type and receiver antenna type are basically based on single-day results, without detailed study and analysis of the relationship. This paper will use GPS as the reference constellation, establish the multi-day continuous ISB solution model, and investigate and discuss the ISB time characteristics between BDS-2 and BDS-3 in the BDS system and between GNSSs.

This study will focus on the short- and long-term time characteristics of multi-GNSS ISBs, as well as the correlation between ISBs and receiver characteristics. The content of this paper is mainly arranged from the following aspects. In the first section, the UDUC PPP model of three systems is derived, the errors involved are elaborated, and the generation mechanism and processing methods of ISB are elaborated. The second section describes the data source and processing strategies. The third section analyzes the ISB time characteristics and the relationship between GNSS, receiver type, receiver antenna type, and ISB. Finally, the summary and prospects are provided.

2. Methods

The formulas used in the mathematical model of multi-GNSS UDUC PPP are discussed. The ISB generation mechanism, parameter composition, and parameter processing strategy in multi-GNSS PPP are analyzed, laying the theoretical foundation for subsequent data analysis.

2.1. Undifferenced and Uncombined Observation Equations

The raw GNSS PPP observation equation can be expressed as follows:

$$P_{r,i}^{s,sys} = \rho_r^{s,sys} + cdt_r^{s,sys} - cdt^{s,sys} + m_r^s \cdot Z_r + \mu_i^{s,sys} \cdot I_{r,1}^{s,sys} + b_{r,i}^{s,sys} - b_i^{s,sys} + e_{r,i}^{s,sys} \quad (1)$$

$$L_{r,i}^{s,sys} = \rho_r^{s,sys} + cdt_r^{s,sys} - cdt^{s,sys} + m_r^s \cdot Z_r - \mu_i^{s,sys} \cdot I_{r,1}^{s,sys} + N_{r,i}^{s,sys} + \varphi_{r,i}^{s,sys} - \varphi_i^{s,sys} + \varepsilon_{r,i}^{s,sys} \quad (2)$$

where the superscript *sys* represents the satellite system, and G, E, and C represent GPS, Galileo, and BDS, respectively; *s*, *r*, and *i* represent the satellite PRN, receiver, and carrier frequency, respectively; $P_{r,i}^{s,sys}$ and $L_{r,i}^{s,sys}$ represent the raw pseudorange and carrier phase in meters; $\rho_r^{s,sys}$ represents the geometric distance from the receiver *r* to satellite *s*; *c* represents the speed of light; $dt_r^{s,sys}$ and $dt^{s,sys}$ represent the receiver and satellite clock offset, respectively; $b_{r,i}^{s,sys}$ and $\varphi_{r,i}^{s,sys}$ represent the pseudorange and phase hardware delay at the receiver end, respectively. $b_i^{s,sys}$ and $\varphi_i^{s,sys}$ represent the pseudorange and phase hardware delay at the satellite end, respectively; $N_{r,i}^{s,sys}$ represents the phase ambiguity parameter; Z_r and m_r^s represent the zenith tropospheric wet delay and the corresponding mapping function, respectively, and the zenith tropospheric dry delay is corrected using the Saastamoinen model; $\mu_i^{s,sys}$ is the ionospheric amplification factor, $\mu_i^{s,sys} = f_1^2 / f_i^2$; $I_{r,1}^{s,sys}$ is the ionospheric delay at the first frequency; $e_{r,i}^{s,sys}$ and $\varepsilon_{r,i}^{s,sys}$ represent the noise of pseudorange and carrier phase observations, respectively. In Equations (1) and (2), we assume that the satellite and receiver antenna phase center offset (PCOs) and variations (PCVs), relativistic effects, Sagnac effects, tidal loads (including solid, polar, and ocean tides), and phase wind up (carrier phase only) have been corrected in accordance with the existing model [27].

It is commonly believed that the pseudorange hardware delay is relatively stable and varies little within a day [28]. Typically, the receiver clock offset calculated by the pseudorange value is used as the initial phase receiver clock offset. Therefore, the pseudorange hardware delays $b_i^{s,sys}$ and $b_{r,i}^{s,sys}$ are absorbed by the receiver clock offset, and the phase hardware delay has obvious time-varying characteristics. At the same time, the ambiguity parameter is strongly correlated with the phase hardware delay, which is difficult to separate, and it is generally assumed that the phase hardware delay remains stable over a certain period of time. Thus, it is generally believed that the phase hardware delay is completely absorbed by the ambiguity parameter, and the time-varying part is absorbed by the receiver clock offset. In order to reduce satellite orbit and clock errors, IGS precision products are used for PPP data processing [29–31].

After incorporating the correction for precision satellite orbit and clock offset into Equations (1) and (2) and linearizing them, the UDUC pseudorange and phase observation equations are expressed as follows:

$$\bar{P}_{r,i}^{s,sys} = u_r^{s,sys} \cdot \Delta x + c\bar{d}t_r^{s,sys} + m_r^s \cdot Z_r + \mu_i^{s,sys} \cdot \bar{I}_{r,1}^{s,sys} + e_{r,i}^{s,sys} \quad (3)$$

$$\bar{L}_{r,i}^{s,sys} = u_r^{s,sys} \cdot \Delta x + c\bar{d}t_r^{s,sys} + m_r^s \cdot Z_r - \mu_i^{s,sys} \cdot \bar{I}_{r,1}^{s,sys} + \bar{N}_{r,i}^{s,sys} + \varepsilon_{r,i}^{s,sys} \quad (4)$$

where $\bar{P}_{r,i}^{s,sys}$ and $\bar{L}_{r,i}^{s,sys}$ represent the observed pseudorange and carrier phase minus the calculated value, respectively; $u_r^{s,sys}$ denotes the Line-of-Sight (LOS) vector of unit length; Δx is the incremental values with respect to the a priori position. After correcting the precision clock offset, the time-varying part of the satellite phase hardware delay has been

eliminated. $\bar{d}t_r^{sys}$, $\bar{N}_{r,i}^{s,sys}$, and $\bar{I}_{r,1}^{s,sys}$ are the receiver clock offset, phase ambiguity parameter, and ionospheric delay after re-parameterization, respectively.

In multi-GNSS UDUC PPP, differences caused by different time datum and coordinate system datum between GNSSs need to be dealt with. In general, there are two approaches. One is to estimate a receiver clock offset parameter for each GNSS system, and the other is to take one GNSS, such as GPS, as the base GNSS and estimate a receiver clock offset for one system and the ISB parameter. The second method is adopted, and GPS is used as the reference GNSS; the ISB parameters between other GNSS systems and GPS are then expressed as follows:

$$ISB_r^{G-sys} = \bar{c}d\bar{t}_r^{sys} - \bar{c}d\bar{t}_r^G \quad (5)$$

When the BDS system is involved, BDS-3 is treated as a new GNSS system. In summary, the observation equation of the GPS/BDS/Galileo combined system can be expressed as follows:

$$\begin{cases} \bar{P}_{r,i}^{s,C_2} = u_r^{s,C_2} \cdot x + \bar{c}d\bar{t}_r^{C_2} + ISB_r^{GC_2} + m_r^s \cdot Z_r + \mu_i^{s,C_2} \cdot \bar{I}_{r,1}^{s,C_2} + e_{r,i}^{s,C_2} \\ \bar{L}_{r,i}^{s,C_2} = u_r^{s,C_2} \cdot x + \bar{c}d\bar{t}_r^{C_2} + ISB_r^{GC_2} + m_r^s \cdot Z_r + \bar{N}_{r,i}^{s,C_2} - \mu_i^{s,C_2} \cdot \bar{I}_{r,1}^{s,C_2} + \varepsilon_{r,i}^{s,C_2} \\ \bar{P}_{r,i}^{s,C_3} = u_r^{s,C_3} \cdot x + \bar{c}d\bar{t}_r^{C_3} + ISB_r^{GC_3} + m_r^s \cdot Z_r + \mu_i^{s,C_3} \cdot \bar{I}_{r,1}^{s,C_3} + e_{r,i}^{s,C_3} \\ \bar{L}_{r,i}^{s,C_3} = u_r^{s,C_3} \cdot x + \bar{c}d\bar{t}_r^{C_3} + ISB_r^{GC_3} + m_r^s \cdot Z_r + \bar{N}_{r,i}^{s,C_3} - \mu_i^{s,C_3} \cdot \bar{I}_{r,1}^{s,C_3} + \varepsilon_{r,i}^{s,C_3} \\ \bar{P}_{r,i}^{s,E} = u_r^{s,E} \cdot x + \bar{c}d\bar{t}_r^E + ISB_r^{GE} + m_r^s \cdot Z_r + \mu_i^{s,E} \cdot \bar{I}_{r,1}^{s,E} + e_{r,i}^{s,E} \\ \bar{L}_{r,i}^{s,E} = u_r^{s,E} \cdot x + \bar{c}d\bar{t}_r^E + ISB_r^{GE} + m_r^s \cdot Z_r - \mu_i^{s,E} \cdot \bar{I}_{r,1}^{s,E} + \bar{N}_{r,i}^{s,E} + \varepsilon_{r,i}^{s,E} \end{cases} \quad (6)$$

In Equation (6), $ISB_r^{GC_2}$, $ISB_r^{GC_3}$, and ISB_r^{GE} represent the ISB between other GNSS systems (BDS-2, BDS-3, and Galileo) and GPS.

2.2. ISB Definition

Different GNSS systems have different coordinate and time references, but MGEX's precision ephemeris clock offset products all use a unified GPS time reference, so it is possible to use MGEX precision products without taking the differences between coordinate and time systems into consideration. However, if different GNSS use different reference satellites, it will still lead to differences in the satellite clock offset of each system. Due to the large differences between different GNSS navigation signals, especially the carrier phase frequency, signal bandwidth, and signal spectrum, and the fact that the receiver must go through different channels when receiving signals, there are different digital/analog filter processing, resulting in differences between different systems of hardware delays within the receiver. The ISB consists of inter-system time errors, receiver hardware delay errors, and some unmodeled pseudorange and phase errors, which primarily affect time errors and are equivalent to the difference between receiver clock offsets for systems with ionospheric-free combined hardware delays [32].

2.3. ISB Parameter Stochastic Model

In multi-GNSS PPP, ISB is typically used as the parameter to be solved lumped with the position parameter, ambiguity parameter, and atmospheric parameter, i.e., the receiver clock offset of each GNSS system is solved independently. In general, ISB parameters are processed in three ways: white noise process, random walk process, and random constant process.

ISB conforms to white noise characteristics, i.e., ISB is a Gaussian distribution with zero mean and variance σ^2 , if its parameters are assumed to be independent of time and adjacent epoch, which is expressed as follows:

$$ISB_r^{sys}(k) \sim N(0, \sigma^2) \quad (7)$$

where k represents the epoch. The white noise process is especially suitable when we do not wish to impose any preconceived notions regarding how the parameters will change. Under the assumption that the ISB fluctuates slightly over time, the ISB behaves as a random walk process, and its function is as follows:

$$ISB_r^{sys}(k) = ISB_r^{sys}(k-1) + \omega_{ISB}, \omega_{ISB} \sim N(0, \sigma_{\omega_{ISB}}^2) \quad (8)$$

The random walk parameter is consistent with the previous epoch, and its variance increases linearly with time

The last is the random constant process, and the function model is as follows:

$$ISB_r^{sys}(k) = ISB_r^{sys}(k-1) \quad (9)$$

It is a special case of a random walk process with zero process noise σ^2 . Zhou et al. analyzed in depth the influence of ISB stochastic modeling on multi-GNSS UDUC PPP [8], revealing that the white noise or random walk processes are ideally suited for ISB estimation [30–35]. Therefore, the white noise process was chosen to estimate the ISB parameters in this paper and the ISB variance of the open-source software GAMP was used as the reference value [36], i.e., $\sigma = 60 \text{ m}/\sqrt{\text{s}}$.

3. Data Sets and Processing Strategies

In order to further investigate the relationship between the ISBs and the precise ephemeris and clock offset, GNSS systems, receiver types, and receiver antenna types, 31 MGEX global tracking stations collected data with a 30 s sampling rate during DOY110–140 in 2021 for the multi-GNSS PPP ISB influence experiment analysis. The Turbo Edit method is used for cycle slip detection in pre-processing [36]. These stations are distributed evenly across the globe and are equipped with different types of receivers and receiver antennas. All selected stations can simultaneously receive observation data from all three GEC systems, and if the average number of observation satellites per system is greater than or equal to four, only the results for the number of satellites more than or equal to 4 be used. Figure 1 illustrates the geographical distribution of the selected MGEX station, with different colors representing different types of receivers. Four receivers, namely JAVAD, LEICA, TRIMBLE, and SEPTENTRIO, are used as examples in this paper to analyze the influence of multi-GNSS PPP ISB experiments. Table 1 displays statistical information regarding the receiver information of the selected station.

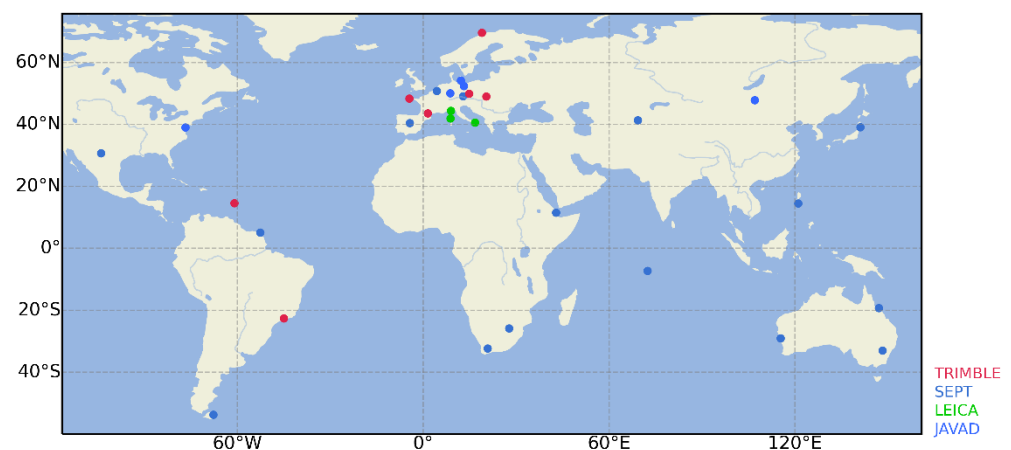


Figure 1. Distribution of the MGEX stations used for the ISB estimation.

Table 1. GNSS receiver information of the selected station.

Manufacturer		Number of Stations (Site Name)
JAVAD	TRE_3	2 (POTS, ULAB)
	TRE_3 DELTA	3 (FFMJ, GODN, WARN)
LEICA	GR30	2 (GENO, MATE)
	GR50	1 (AJAC)
TRIMBLE	NTR9	2 (TRO1, TLSE)
	ALLOY	4 (BRST, CHPG, GANP, LMMF)
	NTR10	1 (GOPE)
SEPTENTRIO	ASTERX4	2 (RIO2, TASH)
	POLARX5	8 (DGAR, DJIG, MDO1, MIZU, PTGG, SUTH, TOW2, YAR3)
	POLARX5TR	6 (BRUX, CEBR, HARB, KOUG, PARK, WTZS)
sum		31

The precision orbit and clock offsets products utilize products from three MGEX analysis centers (Center for Orbit Determination in Europe, Bern, Switzerland (CODE), GeoForschungsZentrum Potsdam, Germany (GFZ), and Wuhan University of China (WHU)), and the data are solved using a continuous static UDUC PPP solution model for multi-day data. All experiments were conducted using self-developed software. PCV correction is not performed for BDS because PCV correction for the BeiDou system is not included in IGS14.atx. Tropospheric wet delay and ionospheric delay were estimated using a random walk process. The ratio of measurement error between pseudorange observations and phase observations was set to 100:1. Table 2 lists specific solution elements in greater detail.

Table 2. Multi-GNSS PPP processing strategy.

Options	Processing Strategies
Observation	UC observation
Signal	BDS: B1, B3; GPS: L1, L2; GAL: E1, E5a
Parameter estimation	EKF
Observation interval	30 s
Weight distribution of observed values	Height angle model
Elevation	7°
Satellite orbit	CODE, WHU, GFZ precise ephemeris
Satellite clock	CODE, WHU, GFZ precise clock offset
Phase center correction	IGS14.ATX
PCV	GPS/Galileo
Phase windup	Model correction
Solid earth tide	
Ocean load	
Polar motion	
Relativistic effect	
Tropospheric delay	Model correction + random walk
Ionospheric delay	Random walk
ISB	White noise
Receiver coordinates	Static, estimated as constants
Receiver clock	White noise estimation
Ambiguity	Estimated as float constants for each arc

4. Experimental Validation

We collected 31 days of data from 110 to 140 days in 2021 for the solution in order to analyze the temporal characteristics of the ISB. The satellite precision orbit and clock offset products from three analysis centers (CODE, GFZ, and WHU) were used to validate and obtain the continuous multi-day results of the ISB from each of the three Analysis Centers (AC). The experimental strategies were as follows: The ISB with GPS as the reference system is obtained by solving with the consecutive day's data. We can obtain 9 sets of ISB time series for each station, depending on how the analysis center products and participating GNSS systems are used. First, the short- and long-term temporal characteristics of the ISB were analyzed, both in terms of the adoption of analysis center products and participation in the GNSS system. Then, consider the effect of day-boundary discontinuous, receiver type, and receiver antenna type on the ISB, i.e., whether the receiver type and receiver antenna type are the same or not same. Finally, the experiment was summarized. In this study, the ISB Root Mean Square (RMS), Standard Deviation (STD), and fluctuation value (maximum minus minimum, FLUC) of single-day and multi-day ISB are used as statistical indicators of the ISB time characteristic change to analyze the relationship between receiver type, receiver antenna type, and ISB. The preceding statistical indicators are abbreviated as Time Characteristic (TC) values for description convenience.

4.1. Analysis of Short- and Long-Term Time Characteristics of ISB

In this section, the short- and long-term time characteristics of ISB are explored and analyzed. For the convenience of nomenclature, the ISB of the three analysis centers are noted as ISB_{COM}^{G-sys} , ISB_{GBM}^{G-sys} , and ISB_{WUM}^{G-sys} , and belong to the same GNSS system, respectively. The ISB between GPS and Galileo, BDS-2, and BDS-3, is expressed as ISB_{AC}^{GE} , ISB_{AC}^{GC2} , and ISB_{AC}^{GC3} , and which use the same analysis center product, respectively. In order to more clearly represent the change of the ISB TC. We shift the ISB time series to the same starting position which has been adopted by Liu and Jiang [32]. This adjustment has no effect on the change in the characteristics of ISBs; it merely modifies the initial position of the ISB time series and has no effect on the analysis of the conclusions regarding the change in the characteristics of ISBs over time. For analysis of the short-term TC of the ISB, the DOY119 ISB results were selected to draw the figure. The daily ISB STD and FLUC for DOY110-DOY140 at the 31 stations were statistically calculated and plotted, and the daily ISB RMS was also calculated and plotted. The STD and FLUC of the ISB time series for 31 days were counted to analyze ISB's long-term TC, and the ISB TCs were then summarized.

4.1.1. Analysis of DBD Effect on Time Characteristics of the ISB

The precise orbit and clocks offset for the WUM, GBM, and COM are estimated daily, so we must deal with the DBD for consecutive days. Satellite orbit DBD can be eliminated, according to Yang et al. [37], but not for satellite clock DBD. Thus, in order to weaken the influence of the DBD on positioning results and the ISB, the algorithm recommended by Yang et al. is used to eliminate the influence of satellite orbit DBD [37]. For satellite clock offset DBD, we adopt the following strategy to weaken its influence: for the sake of description, the last epoch of day D_t is denoted as E_k , and the first epoch of day D_{t+1} is denoted as E_{k0} . The ISB and receiver clock offset of the epoch E_k are used as the initial values of the corresponding epoch E_{k0} , and the normal equation $P_{t,k}$ of E_k is used as the initial normal equation $P_{t+1,k0}$ of E_{k0} . The atmospheric delay of E_{k0} constrains the atmospheric delay of E_k , and the ambiguity $N_{t,k}$ of E_k is used as the initial value of $N_{t+1,k0}$ of E_{k0} . The epoch E_{k0} elevation is set to 10° to weaken the effect of low-elevation satellites, and the IGG3 method is used to degrade the observations with large residuals. We calculate the average values (E, N, U, and ISB) of the last 5 min results on the day D_t and the 5 min results on the day D_{t+1} , respectively, and plot the difference between the two averages, as shown in Figure 2. Figure 2a shows the result without DBD correction, and Figure 2b shows the result after DBD correction. Different colors represent different stations in Figure 2.

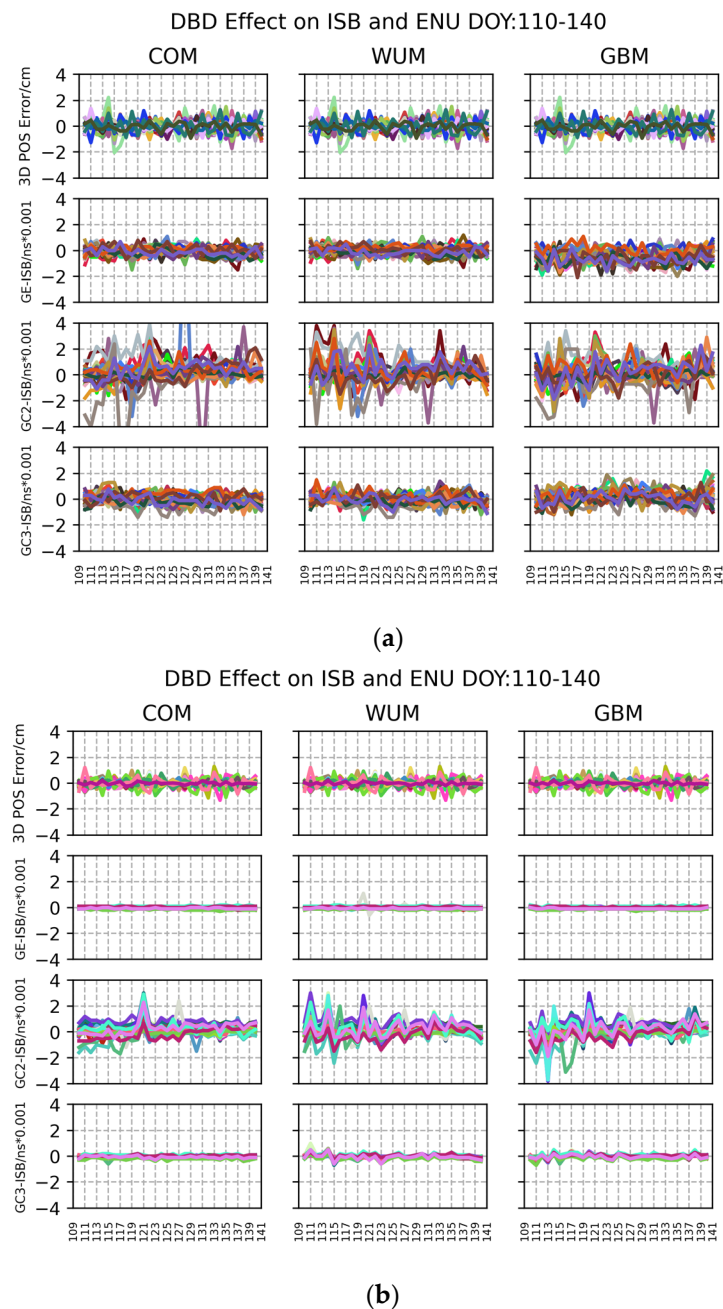


Figure 2. (a). The result without DBD correction at 31 stations (DOY 110-40, 2021). (b). The result of DBD correction at 31 stations (DOY 110-40, 2021).

It can be seen from Figure 2 that the effect of DBD on positioning results is within ± 2 cm, and the effect on ISB is within ± 0.004 ns. The effect of DBD can be weakened after adopting the strategy proposed in this paper, especially for ISB_{AC}^{GE} and ISB_{AC}^{GC3} . However, this DBD effect on ISB is too small to ignore its effect at all. Therefore, the long-term time characteristic changes of ISB will not be affected by adopting the strategy proposed in this paper.

4.1.2. Analysis of Short-Term Time Characteristics of the ISB

Select the ISB results of station AJAC, FFMJ, and PTGG as example plots, as shown in Figure 3. Figure 3a shows the ISB results of DOY119 for the three stations estimated using the products of the three analysis centers. Where the vertical coordinates G-E ISB, G-C2 ISB, and G-C3 ISB indicate ISB_{AC}^{GE} , ISB_{AC}^{GC2} , and ISB_{AC}^{GC3} , and the different colors indicate the ISB

results obtained using different analysis center products. Figure 3b,c shows the daily ISB STD and FLUC for three stations DOY110-140, respectively. The average values of the ISB RMS for 31 days at each of the three stations are displayed in Table 3. Table 4 displays the average values of the ISB STD and FLUC for 31 stations over the course of 31 days. The daily results of the multi-day consecutive data processing results are used as the single-day data processing results in this study for the ISB short-term time characteristic experiments. In this experiment, the RMS, STD, and FLUC of the ISB single-day data processing results are statistically calculated separately, and the average values of the corresponding 31-day single-day data processing results are statistically calculated. For concise presentation, the former is referred to as the ISB short-term TC, whereas the latter is referred to as the ISB monthly average short-term TC.

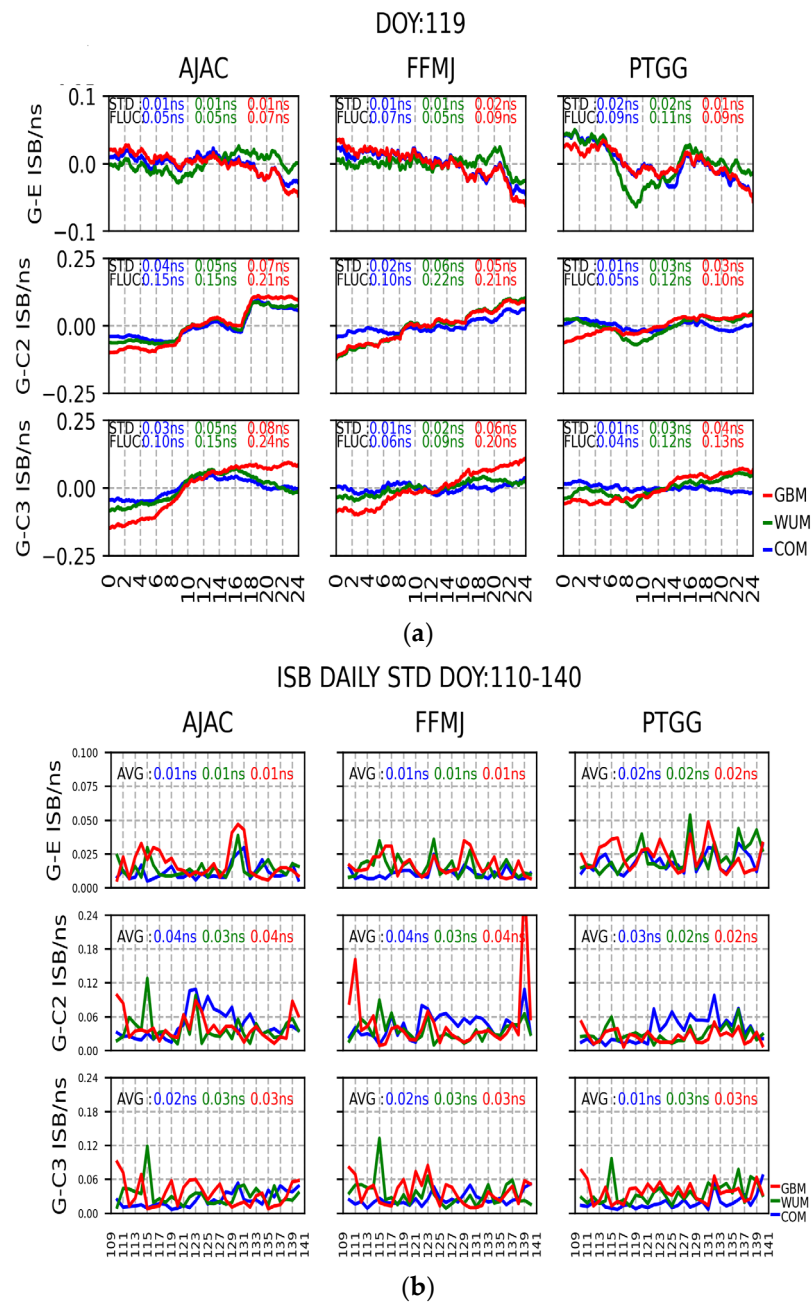


Figure 3. Cont.

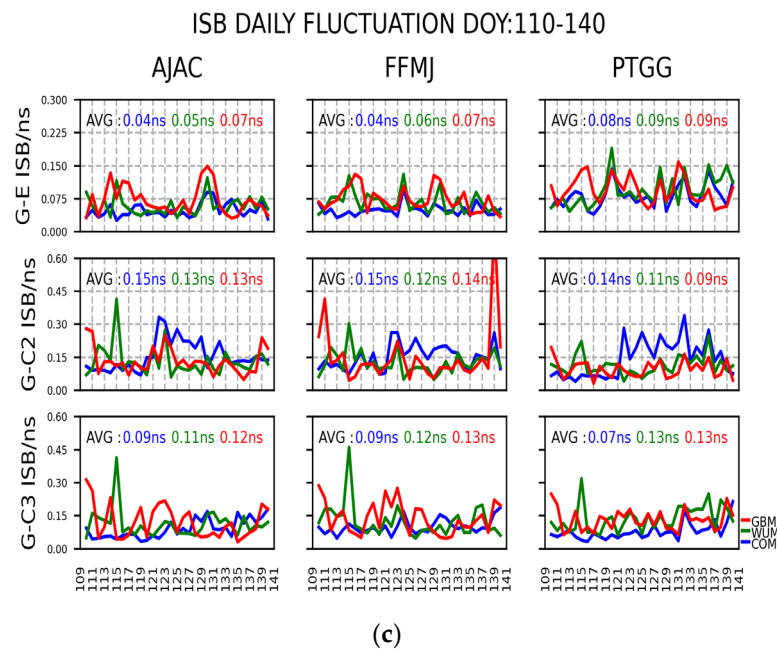


Figure 3. (a). Time series of the ISB at stations AJAC, FFMJ, and PTGG (DOY 119, 2021). (b). Daily ISB STD of station AJAC, FFMJ, and PTGG (DOY 110-140, 2021). (c). Daily ISB FLUC of station AJAC, FFMJ, and PTGG (DOY 110-140, 2021).

Table 3. T Average values of the ISB RMS for stations AJAC, FFMJ, and PTGG (DOY 110-40, 2021).

		RMS/ns		
AC	SITE	ISB^{GE}	ISB^{GC2}	ISB^{GC3}
COM	AJAC	13.54	37.43	38.75
	FFMJ	6.38	16.65	7.95
	PTGG	14.70	43.12	45.71
WUM	AJAC	15.50	42.06	45.69
	FFMJ	8.39	21.50	14.22
	PTGG	16.31	46.60	52.23
GBM	AJAC	8.22	24.74	21.17
	FFMJ	1.05	44.69	52.18
	PTGG	9.57	18.95	13.74

Table 4. T Average values of the ISB STD and FLUC for 31 stations (DOY110-40, 2021).

		ISB STD/ns				ISB FLUC/ns			
AC	COM	WUM	GBM	AVG	COM	WUM	GBM	AVG	
ISB^{GE}	0.01	0.02	0.02	0.02	0.06	0.07	0.08	0.07	
ISB^{GC2}	0.04	0.03	0.04	0.04	0.15	0.12	0.13	0.13	
ISB^{GC3}	0.02	0.03	0.04	0.03	0.09	0.10	0.10	0.10	
AVG	0.03	0.03	0.04	0.03	0.11	0.11	0.13	0.11	

By analyzing the ISB results and combining the result with Figure 3, Tables 3 and 4, the following conclusions can be obtained:

- (1) The ISB_{COM}^{G-sys} , ISB_{WUM}^{G-sys} and ISB_{GBM}^{G-sys} values estimated are not the same because of the differences in data processing strategies used by different analysis centers. ISB_{AC}^{GE} , ISB_{AC}^{GC2} , and ISB_{AC}^{GC3} values are different due to time system differences between GNSS

- systems and receiver hardware delays. Thus, in the short term, the ISB values are correlated with the receiver, GNSS system, the adoption of analysis center products.
- (2) For the ISB_{COM}^{G-sys} , ISB_{WUM}^{G-sys} , and ISB_{GBM}^{G-sys} results, where FLUC was ± 0.25 ns, the monthly average short-term FLUC was ± 0.20 ns, even ISB_{AC}^{GE} was ± 0.10 ns, which can be related to Galileo’s good signal quality. The ISB_{COM}^{G-sys} , ISB_{WUM}^{G-sys} , and ISB_{GBM}^{G-sys} short-term TC show similarity in variation for the same stations. Moreover, it is evident that the ISB TC values of the same GNSS system fall within the same magnitude range. Among the three analysis center products, which use GBM product stability as the worst, COM and WUM are comparable.
 - (3) The short-term FLUC of ISB_{AC}^{GE} , ISB_{AC}^{GC2} , and ISB_{AC}^{GC3} are not the same, but the TC values in the same magnitude. The ISB_{AC}^{GE} , with monthly average short-term ISB STD less than 0.02 ns and FLUC within ± 0.07 ns, shows the best performance. ISB_{AC}^{GC3} performs slightly worse than ISB_{AC}^{GE} , STD less than 0.03 ns and the FLUC is within ± 0.10 ns. The ISB_{AC}^{GC2} is the worst.

4.1.3. Analysis of the Long-Term Time Characteristics of ISB

Figure 4 depicts the ISB RMS time series for each day within 31 days at each station, whereas Table 5 depicts the STD and FLUC of the ISB time series of 31 days for 31 stations. When plotting the single-day RMS of the ISB, the single-day RMS values of ISB_{COM}^{G-sys} , ISB_{WUM}^{G-sys} , and ISB_{GBM}^{G-sys} were adjusted to the same magnitude for ease of analysis by differencing the average RMS values of the respective 31-day ISB time series, which does not affect the analysis of the long-term temporal characteristics of the ISB. In this experiment, the RMS of the ISB data processing results for every day was calculated separately from the STD and FLUC of the ISB data processing results for 31 days, referred to as ISB monthly TC, for the sake of a concise presentation.

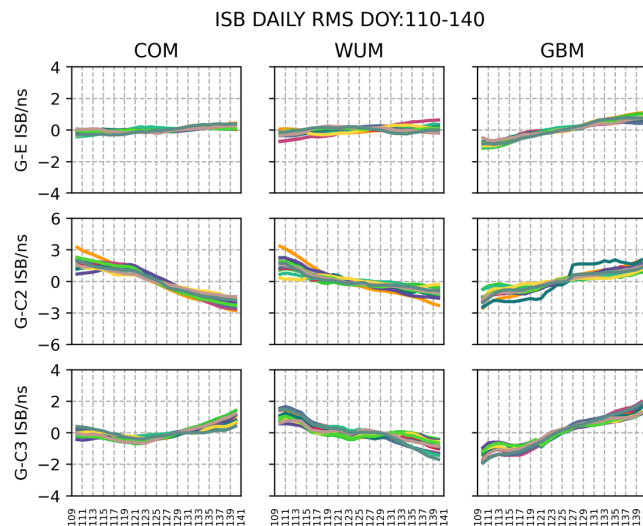


Figure 4. ISB time series at 31 stations, where each color represents a station (DOY110-140, 2021).

Table 5. Long-term STD and FLUC of ISB for 31 stations (DOY110-140, 2021).

AC	ISB STD/ns				ISB FLUC/ns			
	COM	WUM	GBM	AVG	COM	WUM	GBM	AVG
ISB_{AC}^{GE}	0.14	0.12	0.57	0.28	0.45	0.45	1.74	0.88
ISB_{AC}^{GC2}	1.32	0.64	0.69	0.88	3.78	2.33	2.46	2.86
ISB_{AC}^{GC3}	0.40	0.56	0.80	0.59	1.45	2.08	2.64	2.06
AVG	0.59	0.47	0.76	0.61	1.82	1.69	2.58	2.03

The analysis of the short-term TC of the ISB yields a high degree of stability of the ISB parameters in a single day, and the long-term TC of the ISB is analyzed further in this section. Table 5 and Figure 4 clearly present nine sets of ISB time series results over a period of 31 days at 31 stations, clearly reflecting the following conclusions:

- (1) The RMS values of ISB_{AC}^{GE} , ISB_{AC}^{GC2} , and ISB_{AC}^{GC3} are different, as well as the RMS values of ISB_{COM}^{G-sys} , ISB_{WUM}^{G-sys} , and ISB_{GBM}^{G-sys} . Thus, the RMS of the ISBs on different stations, such as ISB_{Sta1}^{GE} , ISB_{Sta2}^{GE} , and ISB_{Sta3}^{GE} , indicates that the ISBs are correlated with receivers, GNSS systems, and adoption of analysis center products in the long term.
- (2) It is clear that the FLUC of ISB_{COM}^{G-sys} , ISB_{WUM}^{G-sys} , and ISB_{GBM}^{G-sys} are not the same, but the TC values between the three are in the same magnitude. The monthly average FLUCs of ISB_{COM}^{G-sys} , ISB_{WUM}^{G-sys} , and ISB_{GBM}^{G-sys} were 1.82 ns, 1.69 ns, and 2.58 ns, corresponding to average STDs of 0.59 ns, 0.47 ns, and 0.76 ns, respectively, where ISB_{WUM}^{G-sys} performed the best, ISB_{COM}^{G-sys} and ISB_{WUM}^{G-sys} were comparable.
- (3) ISB_{AC}^{GE} , ISB_{AC}^{GC2} , and ISB_{AC}^{GC3} long-term TC are not the same. Within 31 days, their monthly average FLUCs were 0.88 ns, 2.86 ns, and 2.06 ns, respectively. The overall ISB monthly average FLUC was 2.03 ns, and the corresponding monthly average STDs were 0.28 ns, 0.88 ns, and 0.59 ns, with an overall monthly average STD < 0.61 ns, ISB_{AC}^{GE} fluctuating the smallest, ISB_{AC}^{GC3} the second, and ISB_{AC}^{GC2} performed the worst.

By analyzing the short- and long-term time series of ISB, it is possible to better understand the error characteristics of ISB, which is crucial for the accurate modeling and rational application of ISB. From the three sets of experiments described above, the following conclusions can be drawn: ISB values correlated with the station receivers, the analysis center products, and GNSS systems. Variations in the short- and long-term TC of ISB_{AC}^{GE} , ISB_{AC}^{GC2} , and ISB_{AC}^{GC3} were not the same. The short-term TC of ISB_{COM}^{G-sys} , ISB_{WUM}^{G-sys} , and ISB_{GBM}^{G-sys} are similar, while not for the long-term. Short-term ISB time series performed better than long-term time series. The DBD effect on ISB can be ignored. ISB_{GBM} performed the worst, while ISB_{COM} and ISB_{WUM} were comparable. In addition, it can be observed that the ISBs have similar long-term time characteristic variations between stations, which will be analyzed in the following section.

4.2. Receiver and ISB Relationship Analysis

In Section 4.1, we investigate and analyze the ISB TC for various ISB time lengths and demonstrate that the ISB TC correlated with the analysis center products and GNSS systems. Meanwhile, many scholars have demonstrated that ISB has a correlation with the type of station's receiver and receiver antenna [16–23], but all are based on single-day results. To investigate the impact of different receiver types and receiver antenna types on ISB for consecutive days, experiments were designed for research and analysis. This paper focuses on four receiver types, namely TRIMBLE, JAVAD, LEICA, and SEPT, and six receiver antenna types, including LEIAR20, SEPCHOKE B3E6, TRM59800.00, etc. In the experiments, 31 station ISB results were selected for plotting, the ISB results of DOY128 days were selected for short-term analysis, the daily ISB RMS of 31 days (DOY110–140) were selected for long-term analysis, and the STD and FLUC of 31 days of ISB results were calculated. According to the previous section, ISB results are correlated with the GNSS system, selected analysis center products, receivers, etc. Thus, the ISB results obtained from various stations are not identical, and the ISB results are de-averaged to facilitate the analysis of the ISB's TC.

Figure 5 shows the ISB results of 31 stations, each equipped with a different receiver type and receiver antenna type, for example, the AJAC station with a LEICA GR50 receiver equipped with TRM115000.00 antenna, the GOPE station with a TPSCR.G3 receiver antenna TRIMBLE NETR9 receiver, etc. The ISB time series of DOY128 and DOY110–140 were analyzed—the ISB results of other stations minus the ISB results of the BRUX station. We

calculated the average STD and FLUC for the 30 stations difference ISB values, as shown in Tables 6 and 7.

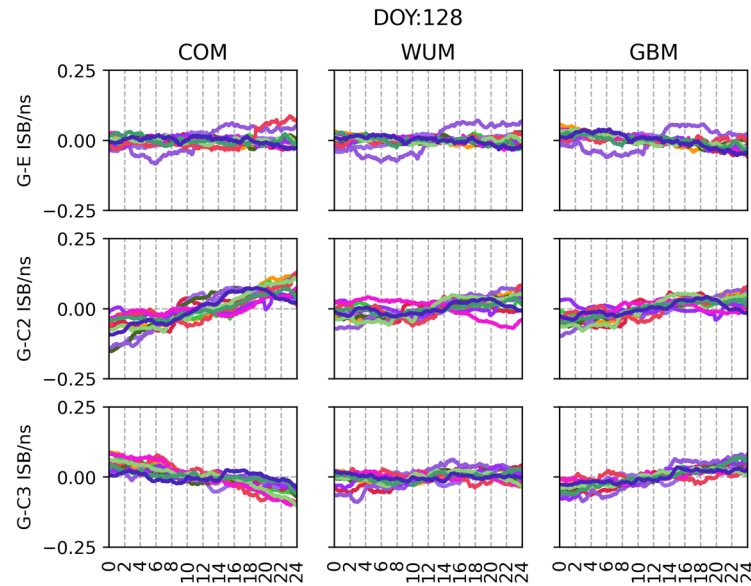


Figure 5. ISB time series at 31 stations, where each color represents a station (DOY128, 2021).

Table 6. Short-term ISB differences between station BRUX and other stations for 31 stations (DOY128, 2021).

AC	ISB STD/ns				ISB FLUC/ns			
	COM	WUM	GBM	AVG	COM	WUM	GBM	AVG
ISB^{GE}	0.0208	0.0205	0.0205	0.0206	0.1100	0.1220	0.1260	0.1193
ISB^{GC2}	0.0351	0.0247	0.0256	0.0285	0.1250	0.1710	0.1840	0.1600
ISB^{GC3}	0.0241	0.0224	0.0253	0.0239	0.0900	0.0919	0.0939	0.0919
AVG	0.0267	0.0225	0.0238	0.0243	0.1083	0.1283	0.1346	0.1238

Table 7. Long-term ISB differences between station BRUX and other stations for 31 stations (DOY110-140, 2021).

AC	ISB STD/ns				ISB FLUC/ns			
	COM	WUM	GBM	AVG	COM	WUM	GBM	AVG
ISB^{GE}	0.1383	0.2122	0.2879	0.2128	0.5400	0.7680	0.7310	0.6797
ISB^{GC2}	0.661	0.8643	0.9217	0.8157	1.9260	2.2100	2.2960	2.1440
ISB^{GC3}	0.2035	0.208	0.2913	0.2343	0.6830	0.7610	0.8600	0.7680
AVG	0.3343	0.4282	0.5003	0.4209	1.0497	1.2463	1.2957	1.1972

In accordance with the previous sections' conclusions, Tables 6 and 7, Figures 4 and 5, it can be known that the ISB is correlated with factors such as the GNSS system and analysis center products for stations with various receiver configurations. In the short-term, Figure 5 demonstrates that the ISB results of the 31 stations fluctuate with the same trend at the macroscopic level, with the difference of ISB FLUC between two stations within ± 0.20 ns and ISB STD less than 0.03 ns, which can be seen in Table 6, and the TC do not show too much difference, especially for ISB_{AC}^{GE} . In the long-term, Figure 4 demonstrates that the ISB TC changes are almost the same for the 31 stations, and the difference of the FLUC is within ± 2.3 ns and STD less than 1.0 ns between stations. This is also consistent with that in Table 7. In conclusion, whether the station equipment receiver type and receiver antenna type are identical, for the ISB results based on continuous processing of multi-day data, the TCs of the ISB had little correlation to receiver type and receiver antenna type.

5. Conclusions

ISB is an essential component of parameter estimation in multi-GNSS PPP data processing; therefore, when different analysis center products are used, multi-GNSS solving must account for the short- and long-term TC change of ISB so that appropriate estimation strategies can be employed. In this paper, the ISB estimation model and the undifferenced and uncombined model of multi-GNSS PPP for GPS, BDS, and Galileo systems are introduced. The TC and parameter estimation methods of the ISB in GPS/BDS/Galileo PPP are investigated. The current status of ISB research is analyzed, as well as the mathematical model of multi-GNSS PPP and the effects of DBD, various analysis center products, receiver types, and antenna types on ISB. Different analysis centers, different combinations of receiver types, and different combinations of receiver antenna types were built and studied to analyze the effects of various ISB combinations. Moreover, the effect of DBD on the long-term time characteristics of ISB was analyzed.

The conclusions made based on the obtained results are as follows:

- (1) ISB is associated with the station receiver type, receiver antenna type, various analysis center products, and GNSS systems.
- (2) Variations in the short- and long-term TC of ISB_{AC}^{GE} , ISB_{AC}^{GC2} , and ISB_{AC}^{GC3} are not the same. The short-term TC of ISB_{COM}^{G-sys} , ISB_{WUM}^{G-sys} , and ISB_{GBM}^{G-sys} are similar, while not for the long-term. The short-term ISB time series performed better than the long-term time series.
- (3) The results of the ISB TC show little correlation between receiver type and receiver antenna. DBD effect on ISB can be ignored for the concussive day's process.

By studying GNSS systems, analysis center products, receiver type, and receiver antenna type in relation to ISB, it is advantageous to analyze the short-term and long-term time variation characteristics of ISB. This aids in a thorough understanding of the error characteristics of ISB and is crucial for the accurate modeling and rational application of ISB. ISB is a significant error term, and its application in PNT is worth further study.

Author Contributions: Y.L. conceived the idea and designed the experiments.; Y.L., B.L. and H.Y. performed the experiments and analyzed the data.; Y.L. wrote the main manuscript.; J.L., B.L., H.Y., A.X. and M.Z., reviewed the paper. All authors have read and agreed to the published version of the manuscript.

Funding: This research was funded by the National Natural Science Foundation of China (Nos. 42030109, 42074012) and the open fund of the State Key Laboratory of Satellite Navigation System and Equipment Technology (CEPNT-2018KF-13) and supported by the Liaoning Revitalization Talents Program (XLYC2002101, XLYC2008034, XLYC2002098).

Data Availability Statement: The datasets analyzed in this study are managed by IGS.

Acknowledgments: All authors gratefully acknowledge CODE, WUM, GFZ, and IGS for providing the data, orbit, and clock products.

Conflicts of Interest: The authors declare no conflict of interest.

References

1. China Satellite Navigation Office BDS System Constellation Status. Available online: <http://www.csno-tarc.cn/system/constellation> (accessed on 20 February 2023).
2. Yang, Y.; Li, J.; Wang, A.; Xu, J.; He, H.; Guo, H.; Shen, J.; Dai, X. Preliminary assessment of the navigation and positioning performance of BeiDou regional navigation satellite system. *Sci. China Earth Sci.* **2014**, *57*, 144–152. [[CrossRef](#)]
3. Yang, Y.; Xu, J. GNSS receiver autonomous integrity monitoring (RAIM) algorithm based on robust estimation. *Geod. Geodyn.* **2016**, *7*, 117–123. [[CrossRef](#)]
4. Wang, J.; Knight, N.L.; Lu, X. Impact of the GNSS Time Offsets on Positioning Reliability. *J. Glob. Position. Syst.* **2011**, *10*, 165–172. [[CrossRef](#)]
5. Yang, Y.; Li, J.; Xu, J.; Tang, J. Generalised DOPs with consideration of the influence function of signal-in-space errors. *J. Navig.* **2011**, *64* (Suppl. S1), S3–S18. [[CrossRef](#)]

6. Teng, Y.; Wang, J. New Characteristics of Geometric Dilution of Precision (GDOP) for Multi-GNSS Constellations. *J. Navig.* **2014**, *67*, 1018–1028. [[CrossRef](#)]
7. Li, X.; Ge, M.; Dai, X.; Ren, X.; Fritsche, M.; Wickert, J.; Schuh, H. Accuracy and reliability of multi-GNSS real-time precise positioning: GPS, GLONASS, BeiDou, and Galileo. *J. Geod.* **2015**, *89*, 607–635. [[CrossRef](#)]
8. Zhou, F.; Dong, D.; Li, P.; Li, X.; Schuh, H. Influence of stochastic modeling for inter-system biases on multi-GNSS undifferenced and uncombined precise point positioning. *GPS Solut.* **2019**, *23*, 59. [[CrossRef](#)]
9. Lou, Y.; Zheng, F.; Gu, S.; Wang, C.; Guo, H.; Feng, Y. Multi-GNSS precise point positioning with raw single-frequency and dual-frequency measurement models. *GPS Solut.* **2016**, *20*, 849–862. [[CrossRef](#)]
10. Chen, J.; Zhang, Y.; Wang, J.; Yang, S.; Dong, D.; Wang, J.; Qu, W.; Wu, B. A simplified and unified model of multi-GNSS precise point positioning. *Adv. Space Res.* **2015**, *55*, 125–134. [[CrossRef](#)]
11. Jiang, N.; Xu, Y.; Xu, T.; Xu, G.; Sun, Z.; Schuh, H. GPS/BDS short-term ISB modeling and prediction. *GPS Solut.* **2017**, *21*, 163–175. [[CrossRef](#)]
12. Li, P.; Zhang, X. Integrating GPS and GLONASS to accelerate convergence and initialization times of precise point positioning. *GPS Solut.* **2014**, *18*, 461–471. [[CrossRef](#)]
13. Bakker, P.; Christian, T. Real-Time Multi-GNSS Single-Frequency Precise Point Positioning. *GPS Solut.* **2017**, *4*, 1791–1803. [[CrossRef](#)]
14. Lu, C.; Li, X.; Cheng, J.; Dick, G.; Ge, M.; Wickert, J.; Schuh, H. Real-time tropospheric delay retrieval from multi-GNSS PPP ambiguity resolution: Validation with final troposphere products and a numerical weather model. *Remote Sens.* **2018**, *10*, 481. [[CrossRef](#)]
15. Mi, X.; Zhang, B.; Yuan, Y. Multi-GNSS inter-system biases: Estimability analysis and impact on RTK positioning. *GPS Solut.* **2019**, *23*, 81. [[CrossRef](#)]
16. Liu, T.; Yuan, Y.; Zhang, B.; Wang, N.; Tan, B.; Chen, Y. Multi-GNSS precise point positioning (MGPPP) using raw observations. *J. Geod.* **2017**, *91*, 253–268. [[CrossRef](#)]
17. Shi, C.; Yi, W.; Song, W.; Lou, Y.; Yao, Y.; Zhang, R. GLONASS pseudorange inter-channel biases and their effects on combined GPS/GLONASS precise point positioning. *GPS Solut.* **2013**, *17*, 439–451.
18. Nadarajah, N.; Teunissen, P.J.G.; Raziq, N. Beidou inter-satellite-type bias evaluation and calibration for mixed receiver attitude determination. *Sensors* **2013**, *13*, 9435–9463. [[CrossRef](#)]
19. Chen, J.; Wang, J.; Zhang, Y.; Yang, S.; Chen, Q.; Gong, X. Modeling and Assessment of GPS/BDS Combined Precise Point Positioning. *Sensors* **2016**, *16*, 1151. [[CrossRef](#)]
20. El-Mowafy, A.; Deo, M.; Rizos, C. On biases in precise point positioning with multi-constellation and multi-frequency GNSS data. *Meas. Sci. Technol.* **2016**, *27*, 035102. [[CrossRef](#)]
21. Torre, A.D.; Caporali, A. An analysis of inter-system biases for multi-GNSS positioning. *GPS Solut.* **2015**, *19*, 297–307. [[CrossRef](#)]
22. Chen, J.; Xiao, P.; Zhang, Y.; Wu, B. GPS/GLONASS System Bias Estimation and Application in GPS/GLONASS Combined Positioning. In *China Satellite Navigation Conference (CSNC) 2013 Proceedings*; Sun, J., Jiao, W., Wu, H., Shi, C., Eds.; Lecture Notes in Electrical Engineering; Springer: Berlin/Heidelberg, Germany, 2013; pp. 323–333. ISBN 978-3-642-37403-6.
23. Dach, R.; Schaer, S.; Hugentobler, U. Combined multi-system GNSS analysis for time and frequency transfer. In *Proceedings of the European Frequency Time Forum, Braunschweig, Germany, 27–30 March 2006*.
24. Gioia, C.; Gaglione, S.; Borio, D. Inter-system Bias: Stability and impact on multi-constellation positioning. In *Proceedings of the 2015 IEEE Metrology for Aerospace, Benevento, Italy, 4–5 June 2015*.
25. Zeng, A.; Yang, Y.; Ming, F.; Jing, Y. BDS–GPS inter-system bias of code observation and its preliminary analysis. *GPS Solut.* **2017**, *21*, 1573–1581. [[CrossRef](#)]
26. Jiao, G.; Song, S.; Chen, Q.; Huang, C.; Su, K.; Wang, Z.; Cheng, N. Modeling and Analysis of BDS-2 and BDS-3 Combined Precise Time and Frequency Transfer Considering Stochastic Models of Inter-System Bias. *Remote Sens.* **2021**, *13*, 793. [[CrossRef](#)]
27. Kouba, J. *A Guide to Using International Gns Service (IGS) Products*; Geodetic Survey Division, Natural Resources Canada: Ottawa, ON, Canada, 2015.
28. Liu, T.; Zhang, B.; Yuan, Y.; Li, Z.; Wang, N. Multi-GNSS triple-frequency differential code bias (DCB) determination with precise point positioning (PPP). *J. Geod.* **2018**, *93*, 765–784. [[CrossRef](#)]
29. Zhang, B.; Teunissen, P.J.; Yuan, Y. On the short-term temporal variations of GNSS receiver differential phase biases. *J. Geod.* **2017**, *91*, 563–572. [[CrossRef](#)]
30. Kouba, J.; Héroux, P. Precise Point Positioning Using IGS Orbit and Clock Products. *GPS Solut.* **2001**, *5*, 12–28. [[CrossRef](#)]
31. Li, B.; Mi, J.; Zhu, H.; Gu, S.; Xu, Y.; Wang, H.; Yang, L.; Chen, Y.; Pang, Y. BDS-3/GPS/Galileo OSB Estimation and PPP-AR Positioning Analysis of Different Positioning Models. *Remote Sens.* **2022**, *14*, 4207. [[CrossRef](#)]
32. Liu, X.; Jiang, W.; Chen, H.; Zhao, W.; Huo, L.; Huang, L.; Chen, Q. An analysis of inter-system biases in BDS/GPS precise point positioning. *GPS Solut.* **2019**, *23*, 116. [[CrossRef](#)]
33. Tu, R.; Hong, J.; Zhang, P.; Zhang, R.; Fan, L.; Liu, J.; Lu, X. Multiple GNSS inter-system biases in precise time transfer. *Meas. Sci. Technol.* **2019**, *30*, 115003. [[CrossRef](#)]
34. Zhang, P.; Tu, R.; Tao, L.; Wang, B.; Gao, Y.; Lu, X. Preliminary Analysis of Intersystem Biases in BDS-2/BDS-3 Precise Time and Frequency Transfer. *Remote Sens.* **2022**, *14*, 4594. [[CrossRef](#)]
35. Blewitt, G. An Automatic Editing Algorithm for GPS data. *Geophys. Res. Lett.* **1990**, *17*, 199–202. [[CrossRef](#)]

36. Zhou, F.; Dong, D.; Li, W.; Jiang, X.; Wickert, J.; Schuh, H. GAMP: An open-source software of multi-GNSS precise point positioning using undifferenced and uncombined observations. *GPS Solut.* **2018**, *22*, 33. [[CrossRef](#)]
37. Yang, H.; Tang, L.; Zhu, H.; Xu, A.; Li, B. A Concise Method for Calibrating the Offset of GPS Precise Satellite Orbit. *Remote Sens.* **2023**, *15*, 8. [[CrossRef](#)]

Disclaimer/Publisher's Note: The statements, opinions and data contained in all publications are solely those of the individual author(s) and contributor(s) and not of MDPI and/or the editor(s). MDPI and/or the editor(s) disclaim responsibility for any injury to people or property resulting from any ideas, methods, instructions or products referred to in the content.